ROYAL SOCIETY OF CHEMISTRY

Check for updates

Isoamylase debranching modified starch and full starch micro/nano fibers prepared by electrospinning†

Xipo Zhao, [ID] *[abc] Min Wang,[ab] Leyao Xu,[ab] Xuankang Li,[ab] Fan Mo,[ab] Chen Tian[ab] and Ling Zhou*[ab]

The high amylopectin content in native starch renders starch solutions suboptimal for meeting the rheological behavior requirements of electrospinning processes, making standalone electrospinning processing particularly challenging. In this work, isoamylase was used to enzymatically modify native starch. Effective debranching was accomplished by using the enzyme's particular activity toward the α-1,6-glycosidic linkages in amylopectin, which produced modified starch with a 57.26% amylose concentration. Electrospinning was employed to fabricate micro/nanofibers from enzymatically modified starch. A systematic investigation was conducted on the electrospinning parameters and morphological characteristics of the resultant micro/nanofibers, successfully producing fibrous structures with diameters ranging from 200–500 nm. This study establishes new methodological references for the application of electrospinning technology in developing all-starch fibrous materials.

1. Introduction

Starch-based fibers, fabricated from starch feedstocks as bio-based green fibrous materials, retain the intrinsic advantages of native starch while exhibiting advantageous characteristics including high porosity, large specific surface area, and low density. These characteristics make them viable substitutes for a variety of traditional polymer fibers. The production of micro/nanofibers from polymer solutions *via* electrospinning technology originated in 1934 when J. Formhals invented an experimental device for polymer fiber fabrication using electrostatic forces and obtained a patent, which is widely recognized as the seminal work of electrospinning based fiber production.[1] The characteristics of electrospun fibers, including their morphology, diameter, alignment, and porosity, can be precisely controlled by modulating processing parameters such as voltage gradient and solution viscosity.[2,3] Notably, Li *et al.*[4] successfully fabricated vertically aligned and high-density single-crystal ultrafine nanofiber bundles through an optimized electrospinning protocol. Hazeri *et al.*[5] employed electrospinning technology to fabricate a blended polymer

nanofibrous scaffold incorporating sulfate groups and polyvinyl alcohol (PVA). This engineered scaffold not only provides biochemical cues essential for stem cell proliferation but also demonstrates neurogenic differentiation induction capabilities. By precisely modulating the composition, topological architecture, and biofunctionality of nanofibers through electrospinning, this approach offers an efficient and controllable solution for neural tissue engineering, exhibiting significant superiority over conventional scaffold fabrication methodologies.

Electrospinning technology demonstrates broad applicability across energy, environmental health, food packaging, and biomedical fields. By precisely modulating nanofiber diameter, morphology, and functionality, it enables tailored material design for target-specific applications. Zhao *et al.*[6] comprehensively reviewed the application of electrospun nanofibrous materials in solar-driven evaporation systems. Owing to their superior properties, including high specific surface area, elevated porosity, tunable architecture, and exceptional flexibility, these materials have gained extensive utilization in solar evaporation. Electrospinning technology enables precise modulation of nanofiber porosity and mechanical strength, thereby providing an ideal substrate for photothermal materials. This optimization facilitates enhanced water transport kinetics and reduced thermal dissipation, ultimately achieving a significant improvement in evaporation efficiency. Wearable Flexible Zinc-Ion Batteries (FZIBs), as a promising energy storage device, are regarded as an ideal alternative to lithium-ion batteries (LIBs) due to their low cost, high safety, and eco-friendliness. Electrospinning technology serves as a robust

[a]Hubei Provincial Key Laboratory of Green Materials for Light Industry, Hubei University of Technology, Wuhan, Hubei 430068, P. R. China. E-mail: xpzhao123@163.com

[b]New Materials and Green Manufacturing Talent Introduction and Innovation Demonstration Base, Hubei University of Technology, Wuhan, Hubei 430068, P. R. China

[c]Hubei Longzhong Laboratory, Xiangyang, Hubei 441000, P. R. China

† Electronic supplementary information (ESI) available. See DOI: https://doi.org/10.1039/d5ra02208h

technique for optimizing component functionalities, significantly enhancing the electrochemical performance and mechanical flexibility of FZIBs, thereby delivering efficient and secure energy solutions for wearable electronic devices.[7]

The application of electrospinning technology in starch fibers originates from the utilization of high-amylose corn starches (Gelose80, Hylon VII, and Hylon V).[8] Researchers are dedicated to optimizing the electrospinning process conditions for pure starch and developing composite fibers by blending starch with other polymers to achieve tailored functionalities, thereby unlocking novel opportunities in textiles, biomedicine, food applications, and related fields.

Natural starch predominantly composed of amylopectin over amylose in its native state develops extensive inter- and intramolecular hydrogen bonding, which facilitates the formation of complex network structures through molecular association. Low water solubility and notable changes in solution viscosity profiles are caused by this structural arrangement, which frequently leads in spontaneous gelation occurrences. The high amylopectin content further imposes steric constraints on molecular mobility, attributed to its branched architecture, where restricted side-chain motion compromises interchain entanglement mechanisms. These combined factors critically impair the rheological behavior required for electrospinnable solutions, particularly manifesting in inadequate viscoelastic properties and insufficient spinnability. As a result, the processability of native starch in electrospinning applications is severely limited.

The linear molecular architecture of amylose molecules facilitates preferential chain alignment, providing adequate spatial allowance for chain segment mobility. Enzymatic modification not only enhances the inherent processability of starch but also elevates amylose content within the system. These structural modifications consequently optimize the entanglement dynamics of starch molecular chains in solution-phase systems, satisfying the rigorous requirements for electrospinnable solution formulation.

Native starch modification involves physicochemical treatments, enzymatic processes, and polymer matrix blending strategies.[9–12] These approaches modify critical structural parameters including molecular chain architecture, granular morphology, and amylopectin/amylose ratio, thereby effectively addressing the inherent processing challenges associated with native starch through material engineering strategies. Enzymatic modification exhibits distinct advantages including mild reaction conditions and environmentally benign characteristics, preventing the solvent residue and pollution issues associated with chemical modification approaches. The enzymatic processing of starch eliminates the requirement for high-pressure or corrosion-resistant equipment, while employing the intrinsic specificity of enzymes to achieve precise hydrolysis with minimal by-product formation, resulting in modified starch products with enhanced safety profiles and biocompatibility.[13,14] Almeida et al.[15] demonstrated that enzymatic treatment of red rice starch with α-amylase and glucoamylase under varied processing conditions significantly reduced amylopectin content. Lee et al.[16] performed isoamylase-mediated

debranching of waxy rice starch and systematically characterizing the crystallinity patterns, yield efficiency, and thermal degradation profiles of debranched starch under controlled thermal regimes. Enzymatic modification of native starch is achieved by precisely modulating key physicochemical properties including viscosity profiles, solubility coefficients, and gelation thresholds. These engineered properties have enabled extensive applications across multiple industrial sectors, particularly in food technology, paper engineering, and textile processing industries.[17–19]

The intrinsic structural characteristics of starch, particularly extensive hydroxyl group-derived hydrogen bonding networks (resulting in compromised solubility) and predominant amylopectin composition (exhibiting limited chain entanglement capacity), render it generally unsuitable for single electrospinning. This fundamental limitation necessitates the incorporation of auxiliary polymeric components to enhance interchain entanglement dynamics within starch-based solutions.[20–23] The regulation of amylose/amylopectin ratios through chemical/physical modifications or linear polymer addition enhances molecular chain entanglement in starch spinning solutions, thereby improving their suitability for electrospinning processes.[24] The selection and modulation of appropriate solvent systems enable the fulfillment of electrospinning requirements for starch-based material systems. Lasprilla-Botero et al.[25] systematically compared the influence of solvent selection on the morphology of electrospun fibers. Due to disparities in solvent electrical conductivity, intrinsic viscosity, and polymer–solvent solubility parameters, significant variations in entanglement concentrations were observed during electrospinning processes. Fibrous membranes with roughened surface topographies exhibited substantially higher water contact angle values compared to smooth-surfaced counterparts. Alonso-González et al.[26] fabricated electrospun fibers from potato starch and rice bran composites using water, formic acid, DMSO, and hexafluoroisopropanol as solvent systems. The study systematically investigated the effects of solution conditions under varying solvents on the morphological characteristics of the hybrid fibers. The results demonstrated that formic acid as the solvent, with a 10% (w/v) rice bran concentration and 40% (w/v) starch concentration, provided optimal electrospinning conditions. This formulation yielded continuous and uniform fibers with 218 ± 89 nm diameter distributions. Sunthornvarabhas et al.[27] dissolved cassava starch in DMSO and PLA in dichloromethane, employing methanol as a co-solvent to facilitate thorough mixing of the two polymer solutions. This solvent engineering strategy successfully fabricated uniform and smooth cassava starch/PLA composite fibers. Sun et al.[28] synthesized starch-graft-polyacrylonitrile (St-g-PAN) graft copolymers in DMSO solvent systems and cerium(IV) as the initiator, with water-soluble starch and acrylonitrile (AN) as monomers. The St-g-PAN composite fibers prepared through electrospinning demonstrated enhanced water resistance, excellent biocompatibility, and enhanced mechanical performance. Xu et al.[29] fabricated acetylated starch (SA) fibers with varying degrees of substitution (DS) in a formic acid/water solvent system. The

fibers demonstrated optimal mechanical performance at DS = 1.1, exhibiting maximum tensile strength of 17.92 MPa in dry state. However, increasing DS to 2.3 resulted in reduced strength (16.19 MPa). Under aqueous environmental, both DS = 1.1 (8.74 MPa) and DS = 2.3 (6.15 MPa) specimens exhibited significantly diminished mechanical properties compared to dry counterparts, attributed to water-induced plasticization effects that disrupt interchain hydrogen bonding between hydroxyl groups in SA fibers. Vasilyev et al.[30] dissolved blends of amylose (AP) and amylopectin (AM) with varying ratios in formic acid to investigate the effects of their composition and aging time on the rheological behavior and spinnability of the solutions. The electrospun fibers exhibited 300–350 nm diameter distributions. Membranes with higher AP content demonstrated brittle fracture behavior, whereas fibers enriched with AM displayed superior mechanical strength. The volatile nature of the organic solvent facilitated controlled evaporation during electrospinning, preventing dripping on the fiber collector and enabling the production of fibers with well-defined morphology, uniform diameter, and enhanced performance.

The electrospinning-mediated fabrication of all-starch-based micro/nanofibers remains underexplored in contemporary research. In this work, native starch was enzymatically modified using isoamylase, leveraging the enzyme's specific activity toward α-1,6-glycosidic bonds in amylopectin to achieve effective debranching and enhance amylose content. Formic acid was employed as the solvent to disrupt hydrogen-bonding networks within starch, enabling complete dissolution and formation of a homogeneous spinning solution. Electrospinning was subsequently utilized to produce enzymatically modified starch micro/nanofibers, with systematic investigation of process parameters and morphological characteristics.

2. Experimental

2.1 Materials

Corn starch (it contains approximately 20% amylose and 80% amylopectin): Wuhan Huali Environmental Technology Co., Ltd. Formic acid (98%, analytical grade): Sinopharm Chemical Reagent Co., Ltd. Isoamylase (activity: 4000 U g^{-1}): Henan Yipin Food Additives Co., Ltd. Citric acid monohydrate (reagent grade); trisodium citrate dihydrate (reagent grade): Sinopharm Chemical Reagent Co., Ltd.

2.2 Enzymatic modification of starch

An appropriate amount of native corn starch and deionized water was weighed. The pH of the deionized water was adjusted to 6.0 using a citric acid–sodium citrate buffer system to prepare starch slurries at concentrations of 10% and 15% (w/v), which were set aside for subsequent use. The starch slurries were then enzymatically modified by reacting with varying quantities of isoamylase for different durations, ultimately yielding enzymatically modified starch suspensions.

The enzymatically modified starch suspension was subjected to centrifugation at 8000 rad min^{-1} for 5 min. Centrifugation was repeated until the supernatant achieved optical clarity. The debranched starch solids were collected and oven-dried to constant mass at 60 °C under forced-air conditions.

2.3 Enzymatic starch modification orthogonal experimental design

Based on preliminary trials, starch slurry concentration was set at 10–20%, enzyme dosage at 60–100 mg, and reaction time at 8–18 days. An orthogonal experimental design was established to determine the optimal conditions, with the orthogonal array provided in Table S1 (see ESI†).

2.4 Preparation of iodine reagent

Accurately weigh 2 g of iodine crystals and 20 g of potassium iodide (KI). Dissolve the solids in deionized water with continuous stirring. Transfer the solution to a 100 mL volumetric flask and dilute to the mark with deionized water to prepare a concentrated stock solution. Subsequently, pipette 10 mL of the stock solution into a second 100 mL volumetric flask and dilute to volume with deionized water, yielding the working iodine reagent (final concentration: 0.02% I$_2$, 2% KI).

2.5 Determination of amylose content

Standard solution preparation: amylose and amylopectin maize starch standard samples (0.1 g each) were accurately weighed, moistened with 1 mL of anhydrous ethanol, and transferred to separate 100 mL volumetric flasks containing 9 mL of 1 mol L^{-1} NaOH. The mixtures were heated in a boiling water bath for 10 min, cooled to ambient temperature, and diluted to the mark with deionized water.

Standard curve construction: calibration standards were prepared in six volumetric flasks by blending amylose and amylopectin reference materials at varying mass ratios. A blank control containing NaOH solution was included. Each solution was sequentially supplemented with deionized water, glacial acetic acid, and iodine reagent diluted to the mark, and allowed to develop color for 10 min. Absorbance values were measured at 620 nm using a UV-Vis spectrophotometer, and a linear calibration curve was established by plotting absorbance against amylose concentration.

Amylose content determination: test samples were accurately weighed and processed identically to the calibration standards. After phase separation via petroleum ether, the target layer was transferred to volumetric flasks. Deionized water, glacial acetic acid, and iodine reagent were sequentially added. Solutions were diluted to volume, allowed to develop color for 10 min, and absorbance was measured at 620 nm. The amylose content of enzymatically modified starch was calculated using the pre-established calibration curve.

2.6 Electrospinning of enzymatically modified starch

The enzymatically hydrolyzed starch was dissolved in formic acid to prepare spinning solutions at concentrations of 10%, 12%, 15%, and 17% (w/v). Each solution was loaded into a 10 mL polyethylene syringe fitted with a stainless steel needle. Electrospinning was performed under controlled parameters:

applied voltages of 10, 15, and 20 kV; feed rates ranging from 0.2 to 1.0 mL h^{-1} (0.2, 0.4, 0.6, 1.0 mL h^{-1}); and a rotating drum collector (aluminum foil-covered, 200 rpm) positioned 8 cm from the needle tip. Environmental conditions were maintained at 30 ± 1 °C and 50 ± 5% relative humidity (RH). The resulting fibers were detached from the collector, vacuum-dried at 60 °C for 12 h to remove residual solvents, and stored in a desiccator prior to morphological characterization. Fiber morphology under varying parameter combinations was systematically analyzed *via* scanning electron microscopy.

3. Characterization

3.1 Ultraviolet spectrum test

The amylose content in enzymatically modified starch was quantified using a UV-Vis spectrophotometer (Model U-3900, China Southern Aviation Industry Co., Ltd). By combining the measured absorbance with the standard curve, the test frequency band was set at 520–720 nm. Each sample was analyzed in triplicate, and the amylose content was calculated by correlating the absorbance values with a pre-established standard calibration curve.

3.2 Enzymatic starch testing and characterization

3.2.1. Fourier transform infrared (FTIR) analysis. The chemical structure of enzymatically modified starch dissolved in formic acid was analyzed using a FTIR spectrometer (Model Bruker 6700, Bruker Corporation, Germany). Measurements were conducted in transmission mode with a spectral range of 400 to 4000 cm^{-1}.

Native corn starch and enzymatically modified starch powder samples were dried in a vacuum drying oven at 60 °C for 24 hours. Test specimens were prepared *via* KBr pelletization and analyzed in transmission mode. Air background signals were subtracted, with 32 cumulative scans acquired over a spectral range of 400–4000 cm^{-1}.

3.2.2. Raman spectroscopy analysis. The structures of the enzymatically hydrolyzed starch and starch fibers were tested using a laser confocal Raman spectrometer (Thermo Fisher Scientific Inc., XploRATMPLUS). The laser wavelength was set at 532 nm, the accumulation time was 10 s, the intensity was 10%, the magnification of the objective lens was 50×, the number of scans was 5, and the test range was 400 to 4000 cm^{-1}.

3.2.3. Rheological behavior analysis. The rheological properties of the starch spinning solution were tested using a high-temperature and high-pressure rotational rheometer (Thermo Fisher Scientific Inc., TDHR-2). The continuous scanning mode under steady state was adopted, and the experimental parameters were set as follows: the angular frequency ranged from 0.1 rad s^{-1} to 1000 rad s^{-1}, and the test temperature was 25 °C.

3.2.4. Scanning electron microscopy analysis. The surface morphology of the samples was observed using a Scanning Electron Microscope (JSM-6390LV, JEOL Ltd, Japan). The starch and starch fibers were attached to the conductive adhesive and subjected to gold sputtering treatment. The test voltage was set

at 3 kV. The scanning images of the electrospun fibers were processed with Image J software to calculate the fiber diameter and its distribution.

4. Results and discussion

4.1 Determination of amylose content in enzymatically hydrolyzed starch

The absorbance of the prepared amylose and amylopectin standard solutions in different proportions was measured. The relationship between the solution concentration and the absorbance was fitted by the least square method, and the standard curve was plotted as shown in Fig. S1.† The regression equation of the standard sample was obtained as: $y = 0.2x + 0.065$, where y is the absorbance of different samples at 620 nm and x denotes the amylose content (%). According to the absorbance of the enzymatically hydrolyzed starch solution measured by the ultraviolet spectrophotometer, the amylose content was calculated from the regression equation.

As shown in Table 1 (orthogonal experiment analysis table) and the orthogonal experimental Table S2,† from the range analysis, it can be obtained that $R_C > R_A > R_B$. During the enzymatic hydrolysis process, the reaction time has the greatest influence on the content of amylose, while the amount of enzyme used has the least influence. Through variance analysis, the optimal conditions were identified as $A_2B_2C_1$, corresponding to a starch slurry concentration of 10% (w/v), isoamylase loading of 80 mg, and reaction time of 18 days.

Isoamylase exhibits specificity by hydrolyzing and breaking the α-1,6-glycosidic bonds in amylopectin. The destruction of amylopectin's branched structure releases more linear amylose molecules. Three parallel experiments conducted under the optimal conditions yielded an average amylose content of 57.26%. This enzymatic modification strategy enables precise regulation of amylose content in starch, which critically governs the viscoelastic properties of electrospinning solutions by modulating molecular chain entanglement density.

4.2 Structure analysis of enzymolysis starch

Fig. 1a shows the infrared spectra of native starch (ST) and enzymatically hydrolyzed starch (EST). In ST, the absorption peak at 3417 cm^{-1} is attributed to the stretching vibration of hydroxyl groups. The abundant hydroxyl groups in starch form a broad and intense absorption peak. The peak at 2926 cm^{-1} corresponds to the asymmetric stretching vibration of –CH$_2$ groups. The 1645 cm^{-1} peak arises from the bending vibration of O–H in residual water molecules within starch. The

Table 1 Orthogonal experiment analysis table

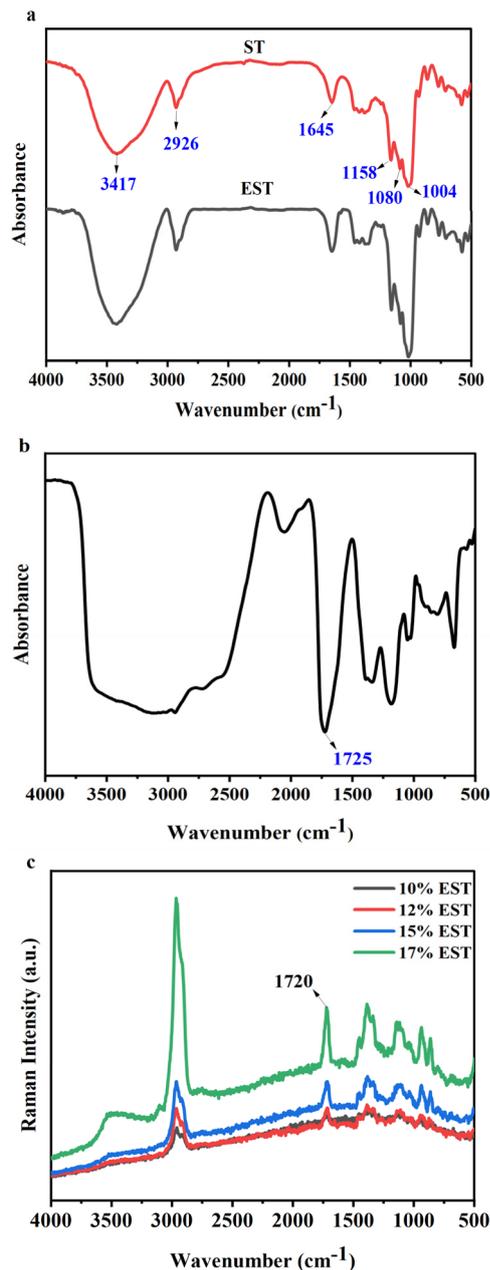|	A	B	C
K1	1.5084	1.495	1.6861
K2	1.5817	1.5237	1.3184
K3	1.3485	1.4199	1.4341
R	0.2332	0.1038	0.3677

Fig. 1 Chemical structural characterization of isoamylase − modified starch and electrospun starch fibers ((a) FTIR spectrum of starch (ST) and enzymatically hydrolyzed starch (EST), (b) FTIR spectrum of enzymatically hydrolyzed starch in formic acid solution, (c) Raman spectra of electrospun samples of enzymatically hydrolyzed starch at different concentrations).

1158 cm^{-1} peak is assigned to the vibration of the C–O group in C–O–H, while the 1080 cm^{-1} peak corresponds to the stretching vibrations of both C–O and C–C bonds. The 1004 cm^{-1} peak is characteristic of the glucose ring vibrations in the starch chains. Notably, the absorption peak positions remain unchanged after direct enzymatic hydrolysis, with no new peaks emerging in EST. This indicates that no chemical reactions occurred during the enzymatic hydrolysis process and no new substances were formed. Fig. 1b shows the infrared spectrum of the starch–

formic acid solution obtained after dissolving enzymatically modified starch in formic acid. The results reveal the appearance of a new ester carbonyl (C═O) absorption peak near 1725 cm^{-1}. This is attributed to the abundant –OH groups on the starch molecular chains, which undergo an esterification reaction with the –COOH groups of formic acid in the solvent, forming formate esters. The emergence of the ester carbonyl peak demonstrates that esterification occurred during the dissolution of enzymatically hydrolyzed starch in formic acid. This observation further confirms that the dissolution of starch in formic acid involves a reactive dissolution process.[31]

As shown in Fig. 1c, with increasing concentration of enzymatically hydrolyzed starch, the Raman scattering intensity gradually increases, and a new Raman peak emerges at 1720 cm^{-1}. This further confirms the formation of formate esters. The progressive enhancement of the ester carbonyl vibration peak with increasing starch concentration indicates that more enzymatically hydrolyzed starch undergoes rapid esterification in formic acid solution.

4.3 Characterization of rheological behavior of electrospinning solution

Fig. 2 reveals that enzymatically hydrolyzed starch solutions in formic acid exhibit shear-thinning behavior across all tested concentrations (10–17% w/v). The shear viscosity gradually increased with starch concentration, displaying an abrupt viscosity transition between 12% and 15%. This viscosity mutation may be attributed to two potential mechanisms. The occurrence of this mutation might be due to the excessively high starch concentration, with physical entanglement formed between the molecular chains, resulting in a sharp increase in viscosity. It could also be that the starch concentration has increased, and formic acid has not completely dissolved the starch, causing the undissolved part to recombine and resulting in a sudden change in viscosity. Notably, even at the lowest concentration (10% w/v), the solution demonstrated a shear viscosity exceeding 100 mPa s at 1000 s^{-1}, satisfying the critical threshold for stable electrospinning. During electrospinning,
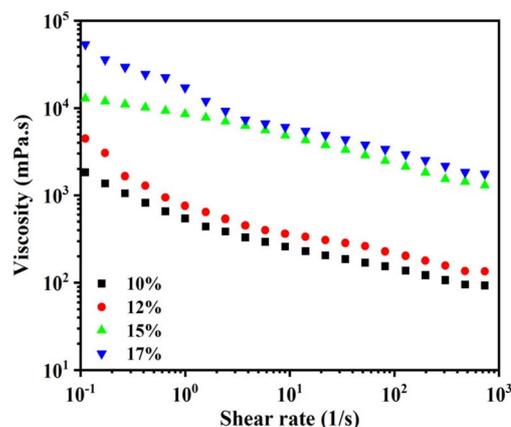
Fig. 2 Rheological curves of formic acid solutions with different concentrations of enzymatically hydrolyzed starch.

the shear rate experienced by the starch solution closely matches the 1000 s^{-1} shear rate used in rheological experiments. To achieve electrospun starch fibers with good morphology, the shear viscosity of the blend dispersion must exceed 100 mPa s at 1000 s^{-1}. Thus, the optimized concentration range for electrospinnable enzymatically modified starch solutions was determined as 10–17% w/v.

This process comprises three sequential stages. Using formic acid as the solvent, its action on starch at room temperature is regioselective, forming monoformate esters at the C6 position of starch glucose units. Due to the high amylose content in enzymatically hydrolyzed starch, the dissolution process in formic acid solution follows three stages as proposed by Lancuski:[32] (1) granule swelling with formylation: starch granules expand while undergoing regioselective formylation at C6 hydroxyl groups. (2) Formate solubilization: the starch formate intermediate dissolves into the formic acid medium. (3) Phase separation & aggregation: the solution evolves from gel-like to liquid-like states and finally forms a biphasic system. Gel-like solutions pose electrospinning challenges due to their high viscosities, which can cause needle clogging during the spinning process.

4.4 Micromorphological analysis of directly enzymatically hydrolyzed starch

Fig. 3 presents the micromorphology of normal corn starch and enzymatically hydrolyzed starch. Panels a–d reveal that different corn starches at the microscale predominantly exhibit irregular spherical structures with smooth surfaces. According to Purwitasari et al.[33] starch derived from Canna edulis treated with thermostable α-amylase exhibited a porous structure. Increasing the enzyme concentration resulted in larger surface pores on the starch granules. This modified starch demonstrated enhanced solubility, oil-absorption capacity, and water-holding capacity compared to native starch. You et al.[18] conducted enzymatic hydrolysis treatment on waxy starch using α-amylase and found that a sponge – like structure with numerous pores formed on the starch surface. After 48 hours of enzymatic hydrolysis, uniform erosion was observed. Fig. 3c and d reveal that the surface of enzymatically hydrolyzed corn starch exhibits a pitted structure. According to the initial stage of starch dissolution in formic acid solution described by Lancuški,[32]

starch granules undergo swelling, thereby facilitating the action of isoamylase on the non-crystalline regions formed by amylopectin molecules within the granules. This enzyme specifically cleaves the α-1,6-glycosidic bonds of amylopectin without hydrolyzing amylose chains. The rough and uneven pitted structures observed in Fig. 3d result from the progressive penetration of isoamylase from the surface into the interior of starch granules, causing localized surface pitting. Despite enzymatic modifications to both the interior and surface regions, the overall structural stability of starch granules is maintained, leading to no significant changes in particle size before and after hydrolysis.

4.5 Micromorphological analysis of electrospun samples

As shown in Fig. 4a, the electrospun morphology of native corn starch at 10% concentration is revealed. Due to the high amylopectin content with extensive branching, the starch solution failed to meet the chain entanglement requirements for electrospinning, resulting in the formation of microspheres and fiber detachment issues. Following isoamylase treatment, the enzymatic hydrolysis specifically cleaved α-1,6-glycosidic bonds in amylopectin, effectively promoting chain entanglement among starch molecules. This structural optimization significantly enhanced fiber formation integrity, as demonstrated in Fig. 4b–e, which exhibit continuous nanofibers with reduced bead defects and improved morphological uniformity.

Combined with the diameter distribution data from Fig. S2 (a′–d′) and Table S3 in the ESI,† it can be observed that increasing the concentration of enzymatically hydrolyzed starch leads to a gradual increase in fiber diameter from 200 nm to 450 nm. Analysis of rheological curves indicates that higher starch concentrations result in increased solution viscosity.
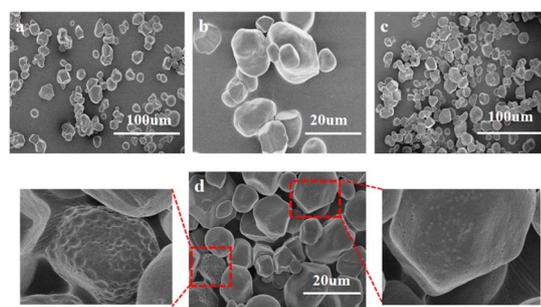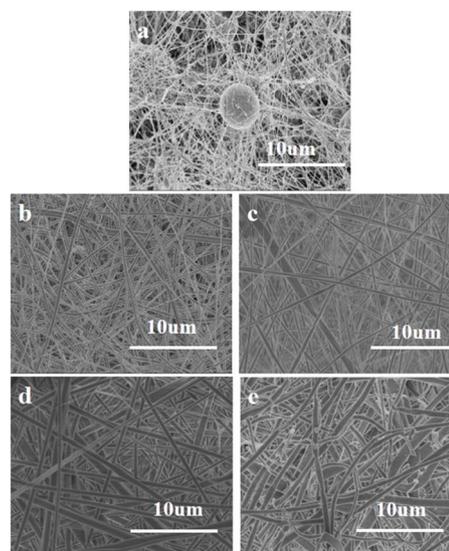

Fig. 4 Electrospun micromorphology of normal corn starch and enzymatically hydrolyzed starch at different concentrations ((a) electrospun normal corn starch at 10% concentration; (b)–(e) electrospun enzymatically hydrolyzed starch samples at 10%, 12%, 15%, and 17% concentrations).
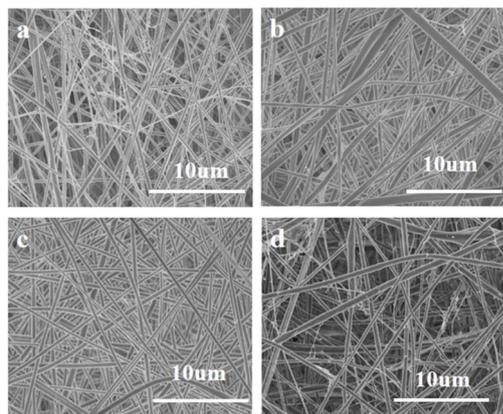

Fig. 3 Micromorphology of different starch powders ((a) and (b) normal corn starch; (c) and (d) enzymatically hydrolyzed corn starch).

Fig. 5 Electrospun micromorphology of 10% enzymatically hydrolyzed starch at different feed rates ((a)–(d) electrospun enzymatically hydrolyzed starch samples at feed rates of 0.2 mL h⁻¹, 0.4 mL h⁻¹, 0.6 mL h⁻¹, and 1 mL h⁻¹).

During electrospinning, high-viscosity solutions are not sufficiently stretched, leading to thicker fiber formation. Additionally, rapid solvent evaporation during stretching causes the fiber surface to solidify quickly, further contributing to the formation of coarse fibers.

Fig. 5 displays the electrospun fiber morphology of 10% enzymatically hydrolyzed starch at different feed rates. According to Fig. S3 (a′–d′) and Table S3 in the ESI,† fiber diameter increases from 200 nm to 300 nm with rising feed rates under fixed starch concentration. At the maximum feed rate (1 mL h⁻¹), Fig. 5d demonstrates pronounced fiber necking and localized entanglement, attributed to two synergistic factors: (1) reduced stretching time: higher feed rates shorten the jet stretching time in the electric field, resulting in insufficient elongation and increased fiber diameter. (2) Incomplete solvent evaporation: formic acid solvent does not have adequate time to fully volatilize, causing fibers to solidify incompletely before deposition on the collector, leading to entanglement formation.

Fig. 6 presents the electrospinning results of 10% enzymatically hydrolyzed starch at different voltages. Combined with Fig. S4 and Table S3 in the ESI,† fiber diameters significantly increases from 300 nm to 600 nm at higher voltages. Fig. 6c highlights the emergence of irregular nodular structures at 20 kV, attributed to two interrelated mechanisms. Increased electrical force: higher voltages enhance the jet's tensile force, leading to jet instability and uneven fiber formation. Reduced solvent evaporation time: accelerated jet velocity under high
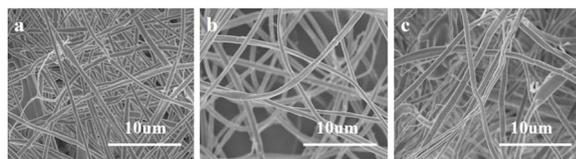
voltage shortens solvent evaporation time, resulting in incomplete solidification and coarser fiber diameters.

5. Conclusions

Starch was enzymatically modified using isoamylase, and orthogonal experiments were employed to optimize modification parameters for enhancing amylose content in starch. The enzymatically hydrolyzed starch achieved an amylose content of 57.26%. Using formic acid as the solvent, enzymatically hydrolyzed starch solutions were prepared, and electrospinning was further applied to fabricate starch micro/nanofibers. By optimizing starch concentration and spinning parameters, starch fibers with diameters ranging from 200–500 nm were successfully produced, providing a novel approach for preparing fully starch-based micro/nanofibers.

Data availability

Data is provided within the manuscript or ESI files.†

Conflicts of interest

There are no conflicts to declare.

References

1 L. Kong and G. R. Ziegler, *FNA*, 2012, **4**, 210–219.
2 Y. Huang, J. Song, C. Yang, Y. Long and H. Wu, *Mater. Today*, 2019, **28**, 98–113.
3 A. M. Al-Dhahebi, J. Ling, S. G. Krishnan, M. Yousefzadeh, N. K. Elumalai, M. S. M. Saheed, S. Ramakrishna and R. Jose, *Appl. Phys. Rev.*, 2022, **9**, 011319.
4 J.-M. Li, *CrystEngComm*, 2017, **19**, 3392–3397.
5 Y. Hazeri, S. Irani, M. Zandi and M. Pezeshki-Modaress, *Int. J. Biol. Macromol.*, 2020, **147**, 946–953.
6 J. Zhao, Z. Liu, S. C. Low, Z. Xu and S. H. Tan, *Adv. Fiber Mater.*, 2023, **5**, 1318–1348.
7 T. Zhang, J. Ju, Z. Zhang, D. Su, Y. Wang and W. Kang, *J. Energy Chem.*, 2024, **98**, 562–587.
8 L. Kong and G. R. Ziegler, *Biomacromolecules*, 2012, **13**, 2247–2253.
9 X. Liu, L. Chen, Q. Dong, Z. Wang, D. Zhang, J. He, Y. Ye, J. Zhou, W. Zhu, Z. Hu, Z. Din, T. Ma, W. Ding and J. Cai, *Int. J. Biol. Macromol.*, 2022, **222**, 868–879.

Fig. 6 Electrospun micromorphology of 10% enzymatically hydrolyzed starch at different voltages ((a)–(c) electrospun enzymatically hydrolyzed starch samples at voltages of 10 kV, 15 kV, and 25 kV).

10 W. Su, Z. Chang, Y. E, Y. Feng, X. Yao, M. Wang, Y. Ju, K. Wang, J. Jiang, P. Li and F. Lei, *Int. J. Biol. Macromol.*, 2024, **263**, 130335.

11 N. Masina, Y. E. Choonara, P. Kumar, L. C. Du Toit, M. Govender, S. Indermun and V. Pillay, *Carbohydr. Polym.*, 2017, **157**, 1226–1236.

12 G. Tan, L. Wang, W. Pan and K. Chen, *IJN*, 2022, **17**, 3913–3931.

13 S. Punia, *Int. J. Biol. Macromol.*, 2020, **144**, 578–585.

14 S. H. Park, Y. Na, J. Kim, S. D. Kang and K.-H. Park, *Food Sci. Biotechnol.*, 2018, **27**, 299–312.

15 R. L. J. Almeida, T. Dos Santos Pereira, V. De Andrade Freire, Â. M. Santiago, H. M. L. Oliveira, L. De Sousa Conrado and R. P. De Gusmão, *Int. J. Biol. Macromol.*, 2019, **141**, 1210–1219.

16 D.-J. Lee, E. Y. Park and S.-T. Lim, *Int. J. Biol. Macromol.*, 2019, **140**, 350–357.

17 B. Zhang, Y. Bai, X. Li, Y. Wang, J. Dong and Z. Jin, *Int. J. Biol. Macromol.*, 2024, **266**, 131234.

18 S. You and M. S. Izydorczyk, *Carbohydr. Polym.*, 2007, **69**, 489–502.

19 P. Liu, L. Ma, W. Duan, W. Gao, Y. Fang, L. Guo, C. Yuan, Z. Wu and B. Cui, *Carbohydr. Polym.*, 2023, **319**, 121183.

20 I. Silva, M. Gurruchaga, I. Goñi, M. Fernández-Gutiérrez, B. Vázquez and J. S. Román, *J. Appl. Polym. Sci.*, 2013, **127**, 1475–1484.

21 J. Gomez-Caturla, J. Ivorra-Martinez, D. Lascano, R. Balart, D. García-García, F. Dominici, D. Puglia and L. Torre, *Polym. Test.*, 2022, **106**, 107462.

22 Q. Liang and Q. Gao, *Food Hydrocolloids*, 2023, **136**, 108250.

23 X. Huang, Z. Teng, F. Xie, G. Wang, Y. Li, X. Liu and S. Li, *Food Hydrocolloids*, 2024, **148**, 109426.

24 Z. Lin, H. Cheng, K. He, D. J. McClements, Z. Jin, Z. Xu, M. Meng, X. Peng and L. Chen, *Food Hydrocolloids*, 2024, **151**, 109860.

25 J. Lasprilla-Botero, M. Álvarez-Láinez and J. M. Lagaron, *Mater. Today Commun.*, 2018, **14**, 1–9.

26 M. Alonso-González, M. Felix and A. Romero, *Processes*, 2024, **12**, 1204.

27 J. Sunthornvarabhas, P. Chatakanonda, K. Piyachomkwan and K. Sriroth, *Mater. Lett.*, 2011, **65**, 985–987.

28 Z. Sun, M. Li, Z. Jin, Y. Gong, Q. An, X. Tuo and J. Guo, *Int. J. Biol. Macromol.*, 2018, **120**, 2552–2559.

29 W. Xu, W. Yang and Y. Yang, *Biotechnol. Prog.*, 2009, **25**, 1788–1795.

30 G. Vasilyev, R. Vilensky and E. Zussman, *Carbohydr. Polym.*, 2019, **214**, 186–194.

31 F. N. D. Santos, E. P. D. Cruz, L. M. Fonseca, J. B. Pires, P. S. Diaz, A. R. G. Dias and E. D. R. Zavareze, *Int. J. Biol. Macromol.*, 2024, **266**, 131182.

32 A. Lancuški, G. Vasilyev, J.-L. Putaux and E. Zussman, *Biomacromolecules*, 2015, **16**, 2529–2536.

33 L. Purwitasari, M. P. Wulanjati, Y. Pranoto and L. D. Witasari, *Food Chem. Adv.*, 2023, **2**, 100152.